Prescribed Pattern Transformation in Swelling Gel Tubes by Elastic Instability

Howon Lee, Jiaping Zhang, Hanqing Jiang, and Nicholas X. Fang

Prescribed Pattern Transformation in Swelling Gel Tubes by Elastic Instability

Howon Lee,[1] Jiaping Zhang,[2] Hanqing Jiang,[2] and Nicholas X. Fang[1],*

[1]Department of Mechanical Engineering, Massachusetts Institute of Technology,

Cambridge, MA 02139, USA

[2]School for Engineering of Matter, Transport, and Energy, Arizona State University,

Tempe, AZ 85287, USA

We present a study on swelling-induced circumferential buckling of tubular shaped gels. Inhomogeneous stress develops as gel swells under mechanical constraints, which gives rise to spontaneous buckling instability without external force. Full control over the post-buckling pattern is experimentally demonstrated. A simple analytical model is developed using elastic energy to predict stability and post-buckling patterns upon swelling. Analysis reveals that height to diameter ratio is the most critical design parameter to determine buckling pattern, which agrees well with experimental and numerical results.

Buckling instability has been studied extensively for the past few decades as one of the most critical structural failure modes [1]. This classical theme is recently gaining new attention as a useful way for creation and transformation of patterns because buckling is often accompanied with large deformation and radical shape change of the structure. Nature has already developed such techniques to leverage mechanical instability to create

a wealth of complex patterns. As biological tissues and organisms grow non-uniformly or under constraints, plane features transform into rich patterns with complexity as found in such examples as wavy edges of plant leaves [2], fine annular patterns in fingerprints [3, 4], and inter-connected creases of brain cortex [5].

This elegant approach to achieve pattern transformation by harnessing mechanical instability has not been much explored until recent progress in material science and manufacturing technologies for soft materials such as elastomers and hydrogels. Particularly, swelling gels have attracted increasing interest because they can actively grow and shrink depending on environmental conditions such as humidity, temperature, and pH [6-8]. Hydrogel-based structures, therefore, can spontaneously create and reversibly pose different patterns via buckling without the need for external load as opposed to classical structural buckling where mechanical force is essential to trigger mechanical instability. This holds great potential in development of self-operating devices with switchable functionalities.

Recently, simple geometries of hydrogel systems have been investigated in this context, including hydrogel layers with different swelling ratio [9, 10], gel strips and disks bound to a hard substrate [11-13], and polymer films with periodic pores [14]. Taking advantage of buckling for pattern formation, however, has not been extended to more diverse shapes and geometries to further explore inspirations from nature where a host of dynamic features are found. Of particular interest in our study is tubular structure with circumferential wrinkles, which is not only geometrically interesting by itself, but also holds crucial physiological significance in biomedical engineering. For example, wrinkled airway of asthmatic bronchiole results from the swollen inner cell layer. Hence,

its topology and corresponding mechanical condition are essential factors to better understand how diseased cells behave and interact with the physiological circumstances [15, 16]. Although numerical and theoretical studies on non-planar geometries such as a tube and a sphere have been reported [17-19], few have been able to create soft tubular structures with well controlled dimensions and constraints due primarily to lack of three-dimensional (3D) fabrication technology for hydrogels. To reproduce complex patterns emerging in such structures has been even more challenging.

Here we present demonstration of controlled pattern transformation of micro-structured tubular gels using swelling-induced circumferential buckling. Principle behind the pattern formation is explained by simple energy analysis and design criteria to control instability pattern is presented. We employed a novel 3D micro-fabrication technology, projection micro-stereolithography (PμSL) [20], to fabricate hydrogel micro tubes, the bottom of which is fixed to impose constraints against swelling as shown in Fig. 1(a). Characteristic dimensional parameters, t, h, and D represent thickness, height, and diameter of the model structure in dry state, respectively. Subjected to the fixed boundary condition on the bottom, the gel develops inhomogeneous stress when allowed to swell. By appropriate selection of dimension, constrained swelling can be made to exhibit buckling instability, causing the circular wall to transform into wrinkled patterns with different wave numbers.

To demonstrate pattern formation, we fabricated tubular gel samples in different dimensions using poly(ethylene glycol) diacrylate (PEGDA) hydrogel (see Supplemental Material [21]). Four groups of samples (**I-IV**) with different levels of normalized thickness t/h were prepared, with group **I** being thicker and group **IV** being more slender.

Each group consists of six samples (**i-vi**) with different levels of normalized height **h/D**, with the sample **i** being shorter and the sample **vi** being taller (see Supplemental Material for physical dimensions of each sample [21]). For swelling experiment, we placed a sample upside down and put in the bath with water covered with oil layer on top as illustrated in Fig. 1(a). Then the sample was brought into contact with water surface for swelling, while base substrate part on which the gel tube was fixed stayed in the top oil layer. In this way, water can diffuse into the tube wall allowing the sample swell before the constraining base relaxes by wetting. Circular tubes transformed into a wide variety of rich patterns as swelling proceeded, and the evolution of the gel morphology was recorded by a charge-coupled device (CCD) camera throughout the course of the experiment (see Movie S1 and Movie S2).

Figure 1(b) presents swelling patterns obtained in the swelling experiment from different samples. Result of the experiment suggests strong connection between the normalized thickness **t/h** and stability, and between the normalized wall height **h/D** and buckling pattern. Samples in group **I** and **II** had tendency to remain stable during swelling, while samples in group **III** and **IV** underwent mechanical instability and transformed into wrinkled patterns. More interestingly, samples with the same normalized height **h/D** transformed into instability patterns with the number of wrinkles close to each other, regardless of the normalized wall thickness **t/h**. The same trend was observed when we repeated the same experiment using hydrogel with different stiffness and swelling ratio, confirming that dimension plays a dominant role in spontaneous buckling in swelling gel. To better understand and generalize this observation, morphology of swelling gel tube is studied via energy analysis. The interface between tubes and substrates have been treated

to achieve very strong bonding in the experiment, which would otherwise influence buckling formation and mode [22]. Therefore, base of the tube is considered as a fixed boundary condition, whereas the rest of the structure is free to swell. When allowed to swell, there are two possible configurations for the swollen tube to adopt in order to accommodate expanded geometry in the original dimension; compression and buckling, as illustrated in Fig. 1(a). The system chooses a shape that minimizes total potential energy. We assume that the entire structure first swells to the fully swollen state and then the bottom end is forced to fit into its original dry dimension. Therefore, fully swollen state is considered as stress-free reference state, and any deformation from it has an elevated potential energy. Although swelling of gel under constraints involves a coupling of elastic and chemical equilibrium, this coupling effect is negligible because the free energy due to the coupling is assumed to be a constant for both compression and buckling configurations, permitting pure elastic consideration. For compressed configuration in which the structure stays stable, the cross-section of the tube remains circular with the radius varying with height. Therefore, increase in potential energy results solely from the in-plane compression of the structure. On the other hand, situation is not as simple in buckled configuration where wrinkled wall undergoes bending in both circumferential and axial direction. We analyze the elastic energy for both configurations to predict stability as well as post-buckling pattern (see Supplemental Material for detailed formulation [21]).

For stable configuration, cross-section of the tube remains circular with the radius being a function of height only. Therefore, increase in potential energy results solely from the in-plane compression of the structure. We assume that radius is linearly varying from the

dry radius, **R** (=**D/2**), at the fixed bottom to the fully swollen radius, *λR*, at the top, where

λ denotes length-wise equilibrium swelling ratio. Since only in-plane compression is

involved, total elastic energy in the stable configuration is obtained as

$$U_{stable} = \frac{1}{24}\pi EDth \cdot b(\lambda),$$ (1)

where E is Young's modulus of the fully swollen gel and $b(\lambda) = (1 - 1/\lambda)^2 (3 + \lambda)$.

Once the structure becomes mechanically unstable, it buckles and creates wrinkles. In

this configuration, the swollen gel fits into confined geometry by posing a wavy shape at

cost of elastic energy. There are two major parts of energy involved in this case. The first

part is the elastic energy due to the wavy bending along the circumferential direction.

This energy contribution increases with buckling mode because the wall undergoes more

bending with large curvature in higher buckling mode. The second part is the elastic

energy due to the deflection of the wall in axial direction. As the gel swells more near its

free upper end than near its confined bottom, the gel wall has to deflect outwards or

inwards in axial direction depending on the position on the wave. This energy

contribution decreases with buckling mode because higher buckling mode results in

smaller wave amplitude in given length, thus less axial deflection is necessary. Therefore,

with the two energy contributions working together, there exists an optimum buckling

mode that gives minimum total potential energy. This argument can be formulated by

assuming sinusoidal wave pattern. Wave amplitude is obtained in a closed form using

approximation for the elliptic integral [23]. The energy due to the circumferential

bending is obtained by integrating local bending energy varying with the curvature on the

sinusoidal wave. The energy due to the axial deflection is modeled as bending of a set of

cantilever beams surrounding the central axis. In this way, total elastic energy for buckled configuration is obtained as an analytical form given by

$$U_{unstable} = \frac{\pi E t^3 h a^2(\lambda)}{D} \left[\frac{11}{140} n^2 + \frac{1}{16(h/D)^4} \cdot \frac{1}{n^2} \right].$$ (2)

where n is a number of waves along the circumference (i.e., buckling mode) and $a(\lambda) = [(2/(3-\lambda))^2 - 1]^{1/2}$. It is interesting to note that two terms are proportional to n^2 and $1/n^2$, respectively. The former is from circumferential bending (lower energy for lower mode) and the latter is from axial deflection (lower energy for higher mode). We find that this opposite dependence on mode number of two energy contributions in (2) brings the system to a certain buckling mode in the event of buckling. Moreover, it is surprising to see that dimensional parameters involved in this competition in the bracket in (2) are h and D only. In other words, other seemingly-important parameters such as t, λ, and E have no impact on the determination of buckling mode. This trend is verified from our experiments shown in Fig. 1(b). Once the tube buckles, the buckling mode does not depend on t, but only on h/D.

Figure 2(a) plots the total potential energy for buckled configuration (2) as a function of h/D for different possible buckling modes. We can clearly see that for each h/D, there is a mode number n which brings the potential energy to the minimum, suggesting corresponding buckling patterns for given dimension. Taking $\partial U_{unstable}/\partial n = 0$ yields

$$\tilde{n} = \frac{0.944}{(h/D)}.$$ (3)

As the actual buckling mode number is an integer, n is either its largest previous or smallest following integer, whichever gives lower potential energy. This is plotted as a step-like function in Fig. 2(a).

Between stable and buckled state, the system chooses the configuration at the lower energy level. Instability index is defined as follows from (1) and (2) to characterize relative magnitude of the energy levels,

$$\gamma = \frac{U_{stable}}{U_{unstable}}\bigg|_{n=\tilde{n}} = \frac{1}{(t/h)^2} \cdot c(\lambda), \tag{4}$$

where $c(\lambda) = (\sqrt{35/11}/6)[b(\lambda)/a^2(\lambda)]$ is a swelling factor increasing monotonically with λ. $\gamma > 1$ means $U_{stable} > U_{unstable}$, thus the system opts to buckle, while $\gamma < 1$ means $U_{stable} < U_{unstable}$, thus the system remains stable. This result implies that stability is determined by the aspect ratio of tube wall t/h and swelling ratio λ, which matches well with the result found in the literature ($\lambda_{cr} = 0.867 \cdot (t/h)^2$) [11]. λ_{cr} required to trigger buckling instability is plotted as a function of the wall aspect ratio in Fig. 2(b), suggesting that slender walled tube becomes mechanically unstable at smaller swelling ratio.

Figure 3(a) is a stability map that can predict both stability and buckling pattern together. With the horizontal and vertical axes representing h/D and t/D, respectively, any tube geometries can be mapped onto this plot. For given equilibrium swelling ratio λ, corresponding critical wall aspect ratio $(t/h)_{cr}$ for instability from (4) can be represented by a straight line drawn from the origin. The shaded area under this line is unstable region where $\gamma > 1$, hence samples fall into this region are expected to buckle. The slope of this boarder line increases with λ, making the unstable region larger. Furthermore, since buckling mode depends only on h/D as shown in (3), the buckling mode number

can be determined based on the horizontal position of the sample on this map. Collectively, stability of the swelling gel tube as well as buckling pattern can be predicted together from this plot.

To validate the theory, samples tested in swelling experiment in Fig. 1(b) are mapped onto the stability map in Fig 3(a). The critical stability line is drawn for $\lambda=1.5$. Samples on the same sloped line (**I-IV**) have the same instability index. Instability indices defined by (4) for each line are 0.25, 0.55, 2.18, and 4.98, respectively, which means that group **I** and **II** above the stability line should remain circular while group **III** and **IV** below the stability line are expected to create wrinkles. This prediction agrees with experimental result shown in Fig. 1(b). Discrepancy is found in only a few cases of **II-(i-iii)** (in the dotted circle) where nonlinear material behavior of gels at high stress is no longer negligible.

From (3), we know that samples aligned on the same vertical line (**i-vi**) should transform into the same buckling mode regardless of t. This was also experimentally observed in Fig. 1(b). Samples on the same column in Fig. 1(b) have the same h/D and their buckling modes are close to each other. The small difference across different groups should come from the thickness effect. For samples with thick wall, in-plane strain energy along the circumferential direction should also be considered, whereas this term is negligible for thin wall tube buckling where only out-of-plane strain energy along the circumferential direction is dominant. The experimental results for buckling mode numbers are plotted in Fig. 3(b). Buckling patterns from samples spanning a wide range of physical dimension collapse well around theoretical prediction obtained from Fig. 2(a). This shows that we demonstrated full control over the pattern of gel tubes formed by mechanical instability.

The pattern formation has also been simulated by finite element method (FEM), which adopts a coupled theory that considers the total free energy of the gel due both to the polymer network deformation and polymer-solvent mixing [24, 25]. The result also shows good agreement with FEM simulation. A set of representative results is shown in Fig. 1(b). See Supplemental Material [21] for detailed finite element analysis and full comparison between experimental and simulation result.

In summary, we have demonstrated well-controlled wrinkle formation of confined hydrogel tube using swelling-induced circumferential buckling. We have also developed a simple theory based on elastic energy and found that key dimensional parameters sensitive to stability and buckling pattern formation are thickness to height ratio and height to diameter ratio, respectively. Our experimental results showed good quantitative agreement with theoretical prediction as well as FEM simulation. Reversible nature of swelling and shrinking of hydrogel further promises unique opportunities to develop versatile devices with tunable properties. We believe our study on buckling of swelling gels will contribute to increasing the breadth of possible application of soft materials in many emerging fields where complex morphologies and dramatic pattern shift are of critical importance, such as tissue engineering and tunable photonic/phononic band gap materials.

ACKNOWLEDGMENTS

[1] S. P. Timoshenko and J. M. Gere, *Theory of Elastic Stability*. (McGraw-Hill, New York, 1961).

[2] E. Sharon, M. Marder and H. L. Swinney, American Scientist **92**, 254-261 (2004).

[3] M. Kücken and A. C. Newell, Journal of Theoretical Biology **235**, 71-83 (2005).

[4] H. Liang and L. Mahadevan, Proceedings of the National Academy of Sciences **106**, 22049-22054 (2009).

[5] S. A. Bayer and J. Altman, *The human brain during the second trimester*. (Taylor & Francis Boca Raton, 2005).

[6] A. Sidorenko, T. Krupenkin, A. Taylor, P. Fratzl and J. Aizenberg, Science **315**, 487-490 (2007).

[7] L. Dong, A. K. Agarwal, D. J. Beebe and H. Jiang, Nature **442**, 551-554 (2006).

[8] D. J. Beebe, J. S. Moore, J. M. Bauer, Q. Yu, R. H. Liu, C. Devadoss and B.-H. Jo, Nature **404**, 588-590 (2000).

[9] V. Trujillo, J. Kim and R. C. Hayward, Soft Matter **4**, 564-569 (2008).

[10] D. Breid and A. J. Crosby, Soft Matter **7**, 4490-4496 (2011).

[11] T. Mora and A. Boudaoud, The European Physical Journal E **20**, 119-124 (2006).

[12] S. J. DuPont Jr, R. S. Cates, P. G. Stroot and R. Toomey, Soft Matter **6**, 3876-3882 (2010).

[13] J. Dervaux, Y. Couder, M.-A. Guedeau-Boudeville and M. Ben Amar, Physical Review Letters **107**, 018103 (2011).

[14] J.-H. Jang, C. Y. Koh, K. Bertoldi, M. C. Boyce and E. L. Thomas, Nano Letters **9**, 2113-2119 (2009).

[15] A. L. James, P. D. Pare and J. C. Hogg, The American review of respiratory disease **139**, 242-246 (1989).

[16] A. E. Redington, Thorax **52**, 310-312 (1997).

[17] D. E. Moulton and A. Goriely, Journal of the Mechanics and Physics of Solids **59**, 525-537 (2011).

[18] B. Li, F. Jia, Y.-P. Cao, X.-Q. Feng and H. Gao, Physical Review Letters **106**, 234301(2011).

[19] Y.-P. Cao, B. Li and X.-Q. Feng, Soft Matter **8**, 556-562 (2012).

[20] C. Sun, N. Fang, D. M. Wu and X. Zhang, Sensors and Actuators A: Physical **121**, 113-120 (2005).

[21] See Supplementary Material at [URL] for the details of the experimental methods, the derivation of the present theory, and the FEM implementation and results.

[22] Q. Wang, L. Zhang and X. Zhao, Physical Review Letters **106**, 118301 (2011).

[23] Y. L. Luke, Mathematics of Computation **22**, 627-634 (1968).

[24] J. Zhang, X. Zhao, Z. Suo and H. Jiang, Journal of Applied Physics **105**, 093522 (2009).

[25] W. Hong, X. H. Zhao, J. X. Zhou and Z. G. Suo, Journal of the Mechanics and Physics of Solids **56**, 1779-1793 (2008).
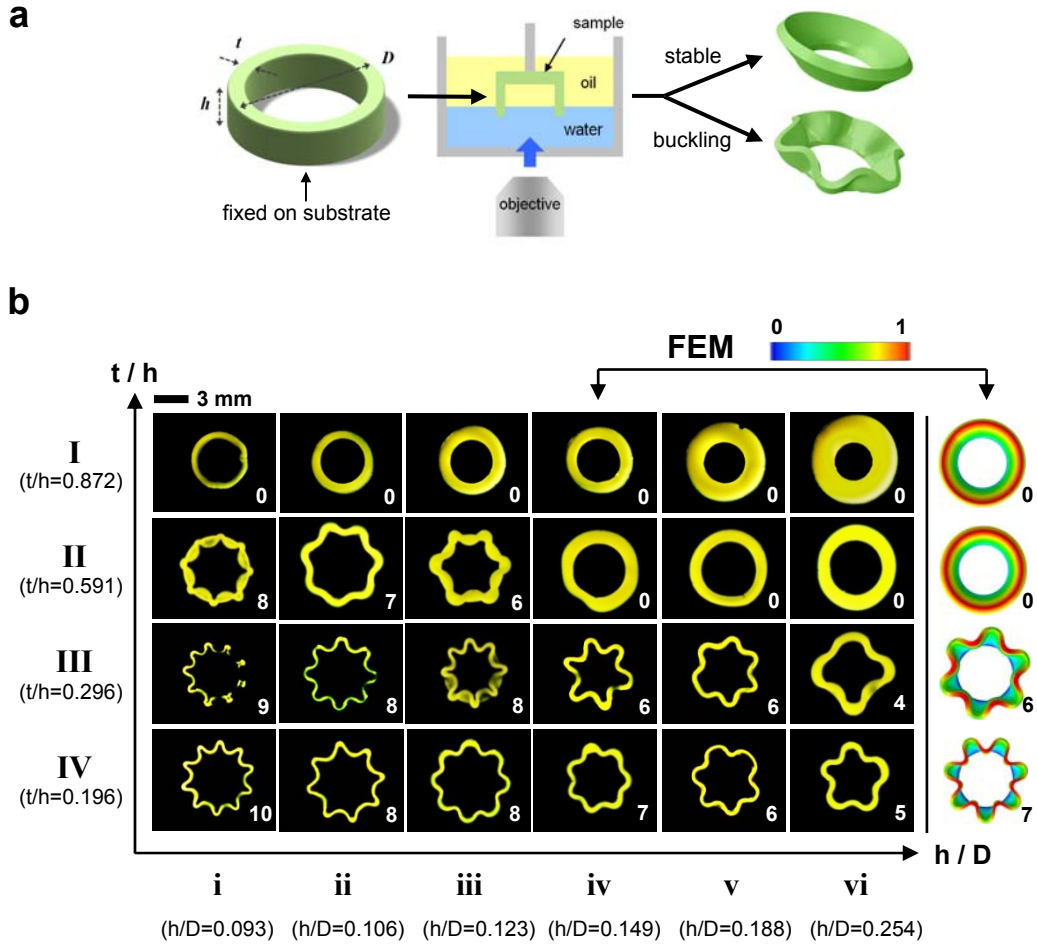
FIG. 1: (Color online) Pattern formation by circumferential buckling of gel tube (a) Characteristic dimensions of tubular gel and experimental setup. (b) Patterns formed in swelling experiment. Samples in the same row have the same *t/h*, and samples in the same column have the same *h/D* (Scale bar indicates 3 mm). Once buckles, the samples in the same row (i.e, with the same *h/D*) show the similar buckling patterns and the samples in the same column (i.e., with the same *t/h*) show the similar stability behavior. FEM simulation result for the group **iv** is also presented showing good agreement with experiment. (Color bar indicates normalized height.)
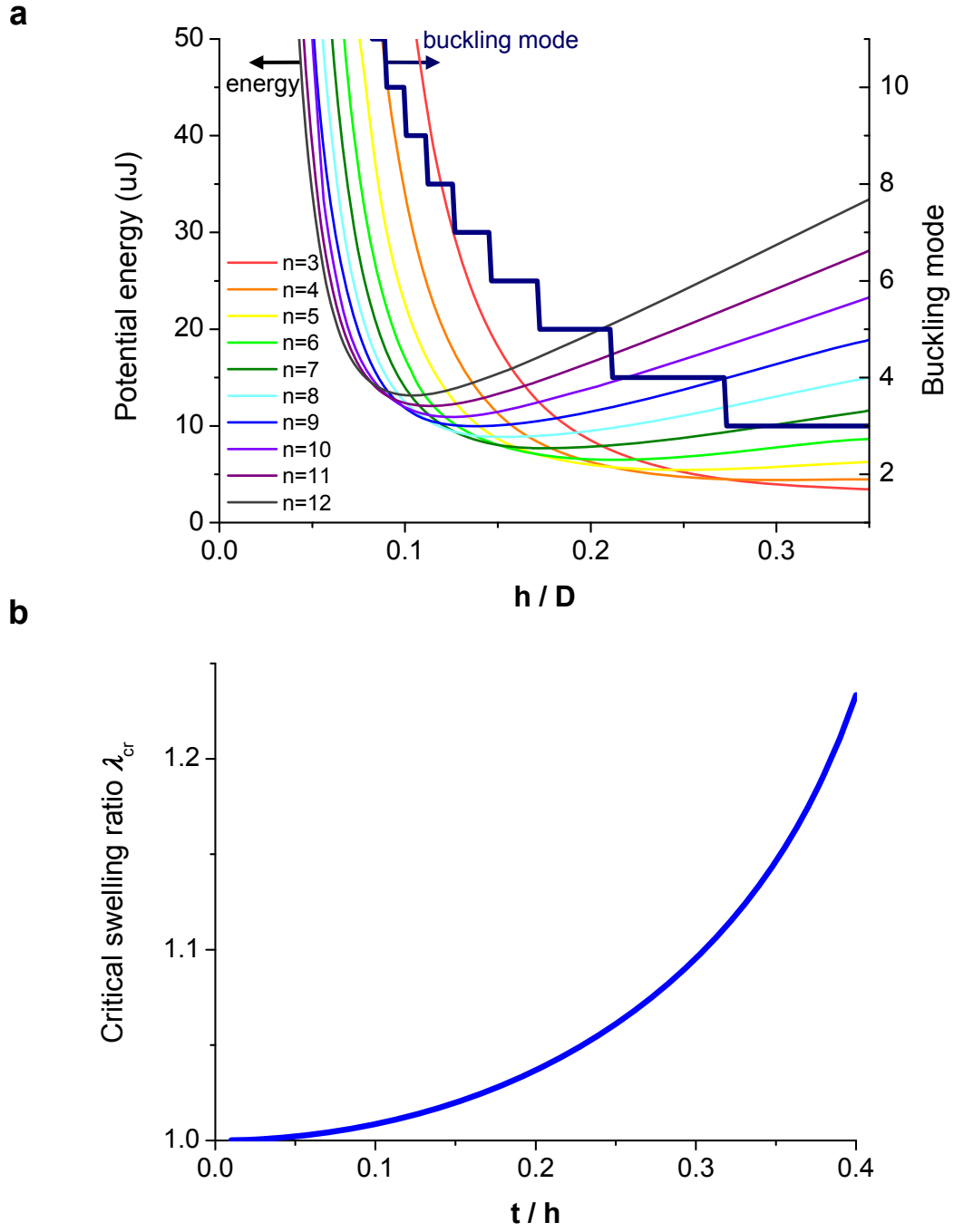
FIG. 2: (Color online) Theoretical prediction (a) Potential energy for different buckling mode. Minimum energy mode varies with **h/D**, resulting in different buckling patterns. (b) Critical swelling ratio for mechanical instability
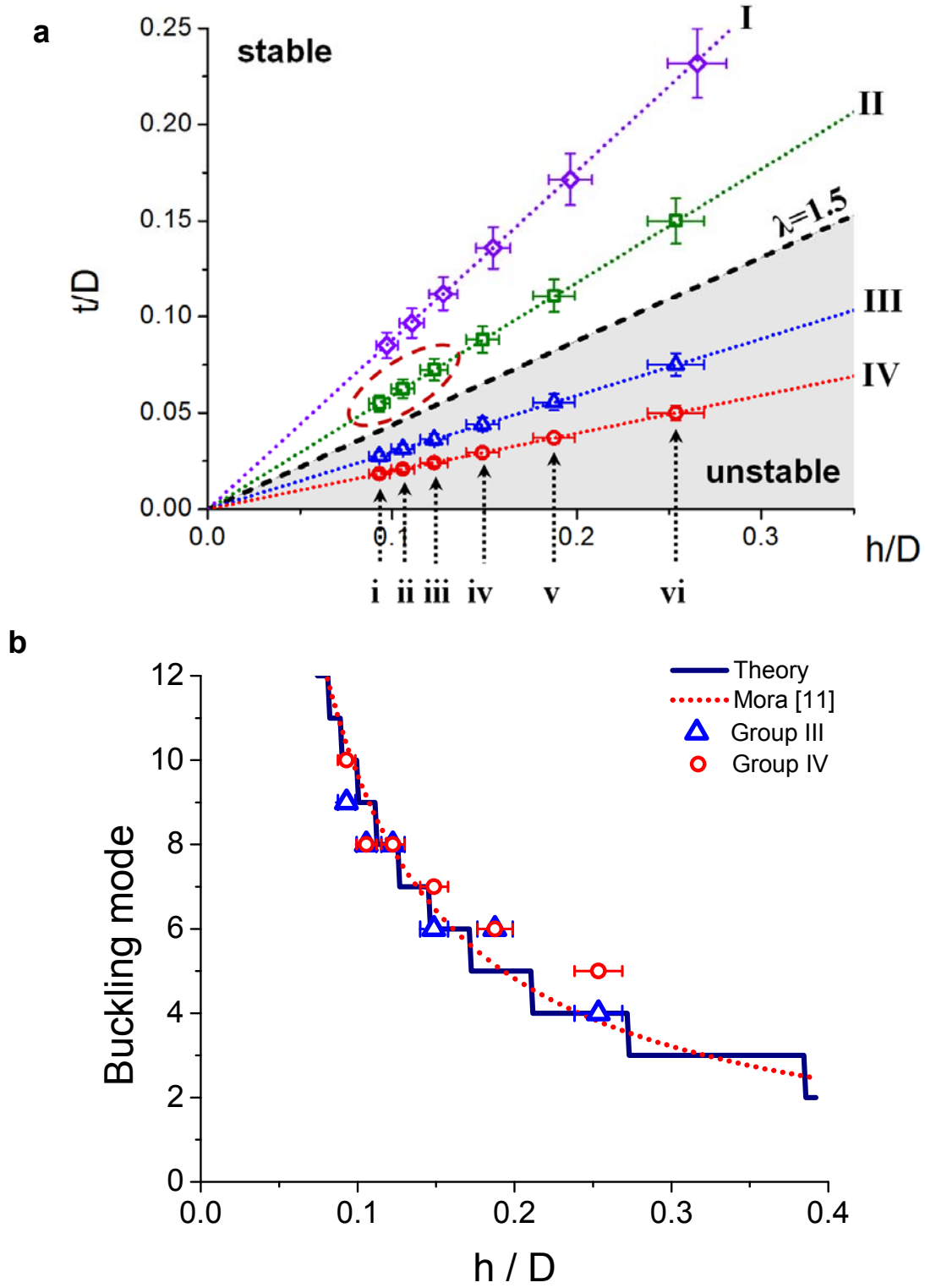
FIG. 3: (Color online) Stability and buckling pattern (a) Critical **t/h** line (dotted) for

λ=1.5 divides upper stable region and shaded unstable region below. Samples shown in

Fig. 1b are grouped into four groups (**I-IV**) by *t/h* for stability and into six groups (**i-vi**) by *h/D* for buckling pattern and are positioned on the stability map. (b) Buckling mode number from unstable samples from experiment. They match well with the prediction by present theory (solid line) as well as the analog of linear elasticity model for strip buckling from the literature (dotted line) [11].